Supporting Information

Synthesis and Characterization of Gold@Gold(I)-Thiomalate Core@Shell Nanoparticles

Gastón Corthey[†], *Lisandro J. Giovanetti*[†], *José M. Ramallo-López*[†], *Eugenia Zelaya*[‡], *Aldo A. Rubert*[†], *Guillermo A. Benitez*[†], *Félix G. Requejo*[†], *Mariano H. Fonticelli*[†,*] *and Roberto C. Salvarezza*[†]

[†]Instituto de Investigaciones Fisicoquímicas, Teóricas y Aplicadas (INIFTA), Universidad Nacional de La Plata - CONICET, Sucursal 4 Casilla de Correo 16 (1900) La Plata, Argentina

[‡]Centro Atómico Bariloche. Comisión Nacional de Energía Atómica, CONICET. Av. Bustillo 9500, Bariloche, 8400 Rio Negro, Argentina.

[*] Corresponding author: mfonti@inifta.unlp.edu.ar

1 UV/Vis Spectroscopy of Reagents and Intermediates

The reagents and intermediates or impurities do not show significant absorption features in the Au plasmon resonance region in the case of Au@Au(I)-TM nanoparticles. It shows that the absorption peak at 520 nm is due to the presence of Au cores.

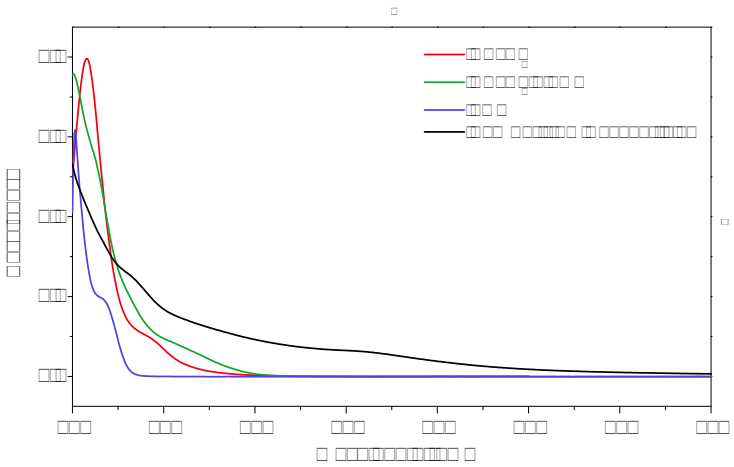

Figure S1: UV/vis spectra of the different components used in the synthesis of the nanoparticles. Red trace: UV/vis spectrum of an aqueous 0.085 mM $HAuCl_4$ solution. Blue trace: 0.13 mM TMA methanolic solution. Green trace: 0.07 mM $HAuCl_4$ + 0.17 mM TMA solution in 15% water and 85% methanol (TMA:Au=2.5). Black trace: As-prepared Au@Au(I)-TM nanoparticles.

2 Transmission Electron Microscopy (TEM)

The size distribution of the nanoparticles was performed using iTEM software.[1] A threshold was defined for each micrograph. Only particles between 1 and 8 nm were considered for the construction of the histogram. A little amount of larger particles were found. Only particles with an aspect ratio close to 1 were considered to avoid counting two close particles as one particle. The average diameter obtained for 580 particles was 3.7 ± 1.3 nm and the histogram is shown in Figure S2c. The histogram was fitted to a Gaussian function.

Dark field (DF) images (Figure S2b) were taken with the objective aperture selecting only a small section of 111 and 200 reflection rings (Figure S2a). It can be observed in the DF image a ring contrast in some nanoparticles. This contrast can be due to the diffuse scattering generated from the top few atomic layers of the nanoparticles, which are affected by reconstruction/relaxation effects (arrow in Figure S2b).[2]

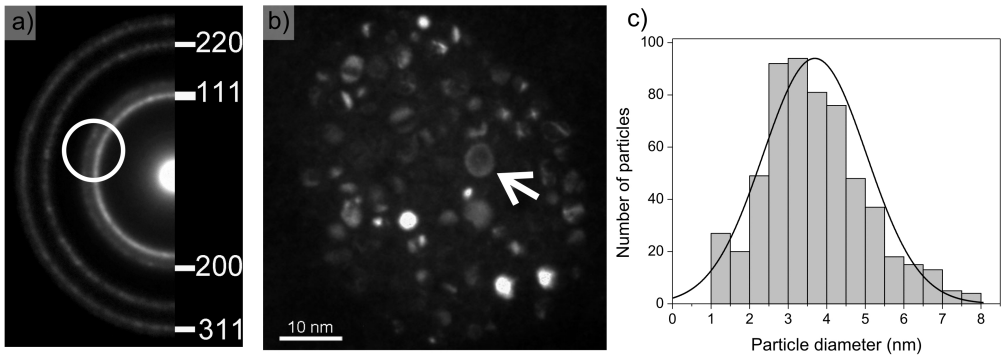

Figure S2: **a)** Diffraction pattern of Au@Au(I)-TM showing the size of the objective aperture used to form the DF image. **b)** DF image of Au@Au(I)-TM nanoparticles. **c)**Histogram of the size distribution of the particles.

Figure S3 shows two High-Resolution TEM (HRTEM) images of two gold nanoparticles along [110] FCC zone axis. The particle in Figure S3a is smaller than the other one S3b. However both particles show sharp sides that could be correlated with a projection of an truncated octahedron (TO) particle.

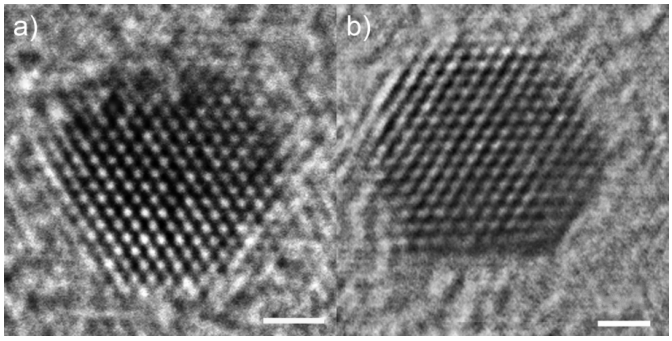

Figure S3: **a)** HRTEM image of Au@Au(I)-TM, scale bar equal to 1 nm. **b)** HRTEM image of a bigger Au@Au(I)-TM particle, scale bar equal to 1 nm.

In order to determine this correlation two particles were simulated with 586 and 1238 atoms respectively. The simulations were performed with JEMS software,[3] using a special routine for particles over an amorphous carbon layer. To better fit the simulations both particles were tilt respect the [110] FCC zone axis 2 degrees. Figure S6a to e show the simulation of a particle with 586 atoms and Figure S4f to j show the simulation of a bigger TO particle with 1238 atoms. It could be notice that the best fit to the particle shown in Figure S4a is reached at a defocus value of 65 nm (Figure S4c) while the best fit for the other particle (Figure S3b) belongs to a defocus value of 145 nm (Figure S4i). The simulation with different quantities of atoms shows a good agreement between the HRTEM

images and the TO particles with a fixed number of atoms.

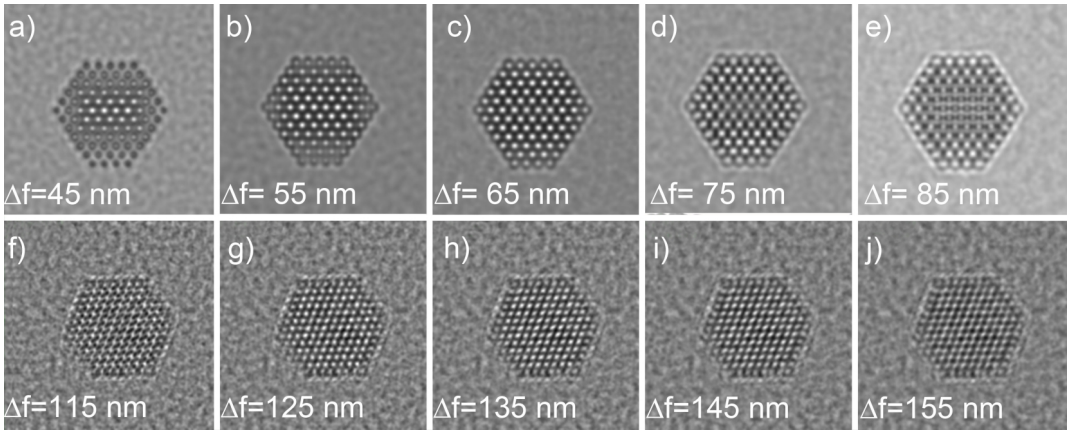

Figure S4: High resolution image simulations of TO particles along [110] FCC axe with 586 atoms (from a to e) and with 1238 (from f to j) respectively. Each figure contains the information of the value for the defocus used in the simulations.

3 Electrochemical reduction of gold on graphite.

Electrochemical measurements were performed using a three-electrode conventional cell with an operational amplifier potentiostat (TEQ-Argentina). The cell was cleaned with piranha solution prior to be use and rinsed with Milli-Q water. A cuasi-reversible hydrogen electrode was used as a reference electrode and a large-area Pt foil as a counter-electrode. All potentials in the text are referred to the Saturated Calomel Electrode (SCE) scale. A highly-oriented pyrolitic graphite (HOPG) substrate was used as a working electrode. Prior to its use, the HOPG was exfoliated, cleaned with aqua regia to remove any metal residue, and rinsed with Milli-Q water. The edges of the HOPG were covered with Teflon. A 1.85 mM $HAuCl_4$ solution was prepared from the stock $HAuCl_4$ solution. Another solution containing 1.85 mM $HAuCl_4$ and 4.6 mM TMA (TMA:Au=2.5) was prepared stirring both components for half of an hour. Every solution was prepared in 0.1 M H_2SO_4 using Milli-Q water. The solutions were degassed with purified nitrogen prior to the experiments. The area of the working electrode informed is the geometric area.

Figure S5 shows the current-potential curves for a HOPG working electrode in the different solutions. The scans were started at 0.9 V in the negative direction at a scan rate of 10 mV/s. The final potential was -0.3 V, where the hydrogen evolution reaction starts. In the case of $HAuCl_4$ solution it was observed a negative current peak at E = 0.62 V, and a current plateau extending from 0.40 V downward to -0.30 V. This limiting current plateau

corresponds to gold electrodeposition from $[AuCl_4]^-(aq)$ according to the reaction:[4]

$$[AuCl_4]^-(aq) + 3e^- \rightarrow Au(s) + 4Cl^-(aq) \quad (1)$$

In the case of the TMA containing solution, a negligible current was observed. These results show that it is very difficult to reduce the Au(I)-TM complex, which explains its partial reduction during the nanoparticle synthesis, even when a 10-fold excess of $NaBH_4$ was used.

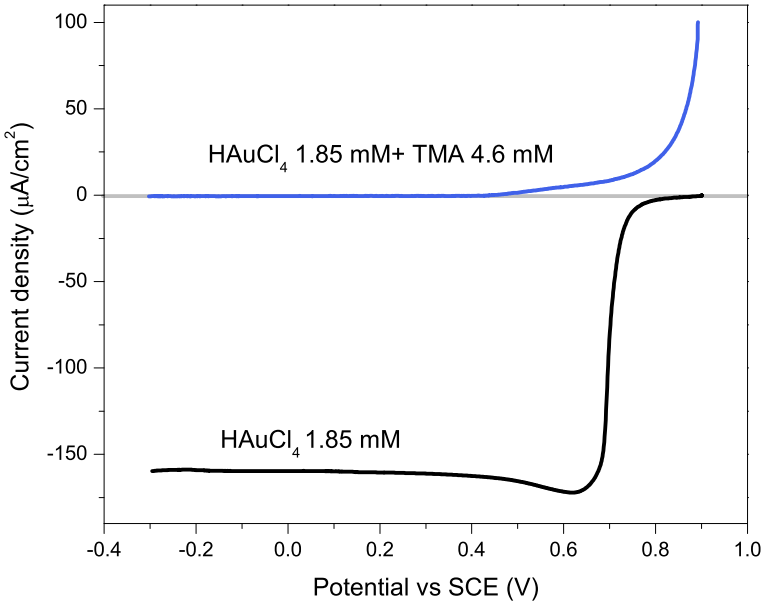

Figure S5: Current density vs potential plot for gold electrodeposition on HOPG from an aqueous 1.85 mM $HAuCl_4$ + 0.1 M H_2SO_4 solution (black trace) and from a 1.85 mM $HAuCl_4$ + 4.6 mM TMA (TMA:Au=2.5) + 0.1 M H_2SO_4 solution (blue trace). Scan rate: 10 mV/s.

4 Reduction of Au(I)-Thiomalate by $NaBH_4$

As shown in this work, it was not possible to completely reduce Au(I)-TM with $NaBH_4$. Here it is proposed that $NaBH_4$, and also weak reducing agents, provides enough driving force for the Au(I) reduction. Hence, a kinetic hindrance might be the responsible for the stability of Au(I)-TM towards reduction.

The formation of $Au(I)-RS$ follows the reaction:

$$Au^+ + SR^- \rightarrow Au(I)-SR \quad \Delta G_f^\circ = -RT\ln(K_{f,Au(I)-RS}) \quad (2)$$

where SR^- represent the thiomalate ions. Then, this compound forms oligomer units

$$n[\mathrm{Au(I)-SR}] \rightarrow [\mathrm{Au(I)-SR}]_n \quad \Delta G^{\circ}_{polymer} = -RT\ln(K_{polymer}) \tag{3}$$

Although the $K_{f,\mathrm{Au(I)-RS}}$ value has already been reported, there were no reports regarding the $K_{polymer}$ value. For this reason, some approximations will be done to estimate the thermodynamic quantities related to Au(I). If the addition of any polymer unit, $\mathrm{Au(I)-RS}$, implies the formation of a Au-S bridge, it could be proposed that for the release of a sulfur free Au(I) specie, two Au(I)-S bonds have to be broken. If any bond breaking has an equilibrium constant of $1/K_{f,\mathrm{Au(I)-RS}}$, a process which implies the consecutive breaking of two Au-SR bonds would be described approximately by $(1/K_{f,\mathrm{Au(I)-RS}})^2$.

$$\begin{aligned}
[\mathrm{Au(I)-SR}]_n &\rightarrow [\mathrm{Au(I)-SR}]_{n-1} + \mathrm{Au(I)-SR} \\
\mathrm{Au(I)SR} &\rightarrow \mathrm{Au(I)} + \mathrm{RS^-} \\
\hline
[\mathrm{Au(I)-SR}]_n &\rightarrow [\mathrm{Au(I)-SR}]_{n-1} + \mathrm{Au(I)} + \mathrm{RS^-} \quad \Delta G^{0}_{diss} = -RT\ln(1/K_{f,\mathrm{Au(I)-RS}})^2
\end{aligned} \tag{4}$$

4.1 Au(I) Reduction Half-Reaction

$$\begin{aligned}
[\mathrm{Au(I)-SR}]_n &\rightarrow [\mathrm{Au(I)-SR}]_{n-1} + \mathrm{Au(I)} + \mathrm{RS^-} & \Delta G^{\circ}_{diss} &= -RT\ln(1/K_{f,\mathrm{Au(I)-RS}})^2 \\
\mathrm{Au^+} + e^- &\rightarrow \mathrm{Au} & \Delta G^{\circ}_{\mathrm{Au^+/Au^0}} &= -FE^{\circ}_{\mathrm{Au^+/Au^0}} \\
\mathrm{RS^-} + \mathrm{H^+} &\rightarrow \mathrm{RSH} & \Delta G^{\circ}_{diss,\mathrm{RSH}} &= -RT\ln(1/K_{\mathrm{a,RSH}}) \\
\hline
[\mathrm{Au(I)-SR}]_n + e^- + \mathrm{H^+} &\rightarrow [\mathrm{Au(I)-SR}]_{n-1} + \mathrm{Au} + \mathrm{RSH} & \Delta G^{\circ}_{red,m} &= \Delta G^{\circ}_{diss} + \Delta G^{\circ}_{\mathrm{Au^+/Au^0}} + \\
& & & \Delta G^{\circ}_{diss,\mathrm{RSH}}
\end{aligned} \tag{5}$$

$$\Delta G^{\circ}_{red,m} = -[RT\ln(1/K_{f,\mathrm{Au(I)-RS}})^2 + FE^{\circ}_{\mathrm{Au^+/Au^0}} + RT\ln(1/K_{\mathrm{a,RSH}})] \tag{6}$$

For TMA, $pK_{a,1}$ = 3.30, $pK_{a,2}$ = 4.94 and $pK_{a,3}$= 10.64.[5] Hence, at pH = 8 both carboxylic groups are as carboxylates while the SH group remains protonated. $K_{a,3}$ is the one related to the reaction $\mathrm{RSH} \rightarrow \mathrm{RS^-} + \mathrm{H^+}$. The $\mathrm{Au(I)-RS}$ (with RS = thiomalate) complex formation constant is $K_{f,\mathrm{Au(I)-RS}} = 1.86 \times 10^{10}$ [6] and $E^{\circ}_{\mathrm{Au^+/Au^0}}$ = 1.692 V.[7] Then, $\Delta G^{\circ}_{diss} = 1.17 \times 10^5$ J mol^{-1} and $\Delta G^{\circ}_{red,m} = -1.07 \times 10^5$ J mol^{-1}. The standard reduction potential, $E^{\circ}_{red} = -(\Delta G^{\circ}_{red,m}/nF)$ is: $E^{\circ}_{red} = 1.1$ V vs. the standard hydrogen electrode (i.e 0.86 V vs. SCE). Considering this figure it is clear that Au(I) is thermodynamically unstable in the presence of mild reducing agents. In the following, the reaction with BH_4^-, a strong reducing agent, is considered.

4.2 $NaBH_4$ Oxidation Half-Reaction

$NaBH_4$ is hydrolyzed in water following the reaction:

$$\mathrm{NaBH_4 + 4H_2O \rightarrow H_3BO_3 + NaOH + 4H_2} \tag{7}$$

Since the pK_a of boric acid (H_3BO_3) at 20°C is 9.27, at pH=8 (the pH after loading $NaBH_4$ in the nanoparticle synthesis) the boric acid main contributing specie is $B(OH)_3$. Then, $E^\circ_{B(OH)_3/BH_4^-} = -0.481$ V.[7]

$$\mathrm{BH_4^- + 3H_2O \rightarrow B(OH)_3 + 7H^+ + 8e^-} \quad \Delta G^\circ_{ox} = 8FE^\circ_{BH_4^-/B(OH)_3} \tag{8}$$

4.3 Complete Redox Reaction

$$\begin{array}{ll} 8\times([\mathrm{Au(I)-SR}]_n + e^- + \mathrm{H^+} \rightarrow [\mathrm{Au(I)-SR}]_{n-1} + \mathrm{Au + RSH}) & 8\times G^\circ_{red,m} \\ \mathrm{BH_4^- + 3H_2O \rightarrow B(OH)_3 + 7H^+ + 8e^-} & \Delta G^\circ_{ox} = 8FE^\circ_{BH_4^-/B(OH)_3} \\ \hline 8[\mathrm{Au(I)-SR}]_n + \mathrm{H^+ + BH_4^- + 3H_2O \rightarrow 8[Au(I)-SR]_{n-1} + 8Au + 8RSH + B(OH)_3} & \Delta G^\circ_{total} \end{array}$$

$$\begin{aligned} \Delta G^\circ_{total} &= 8\times\Delta G^\circ_{red,m} + \Delta G^\circ_{ox} \\ &= -8\times[RT\ln(1/K_{f,\mathrm{Au(I)-RS}})^2 + FE^\circ_{Au^+/Au^0} + RT\ln(1/K_{a,\mathrm{RSH}})] + 8FE^\circ_{BH_4^-/B(OH)_3} \end{aligned} \tag{9}$$

Then, $\Delta G^\circ_{total} = -1.2\times10^6$ J mol^{-1}, which shows that the $[\mathrm{Au(I)-RS}]_n$ reduction by $NaBH_4$ is thermodynamically favorable under standard conditions. The $\mathrm{Au(I)-RS}$ reduction was carried out with $BH_4{}^-$–excess, i.e. a reaction quotient smaller than one, both in the synthesis and in the post-reduction treatment. Furthermore, the polymer reduction was not fast when carried out electrochemically at pH $\approx$ 1.

5 Stability of Au@Au(I)-TM nanoparticles

A sample of as-prepared Au@Au(I)-TM nanoparticles was stored dispersed in water at 4°C for seven months. The XPS spectra of Au 4*f* and S 2*p* are shown in Figure S6. The Au 4*f* signal present the same components as the freshly measured samples with two components already explained in the text. The S 2*p* signal presents an additional component at 167-168 eV. This signal could be ascribed to sulfur species oxidated during the period of storage.

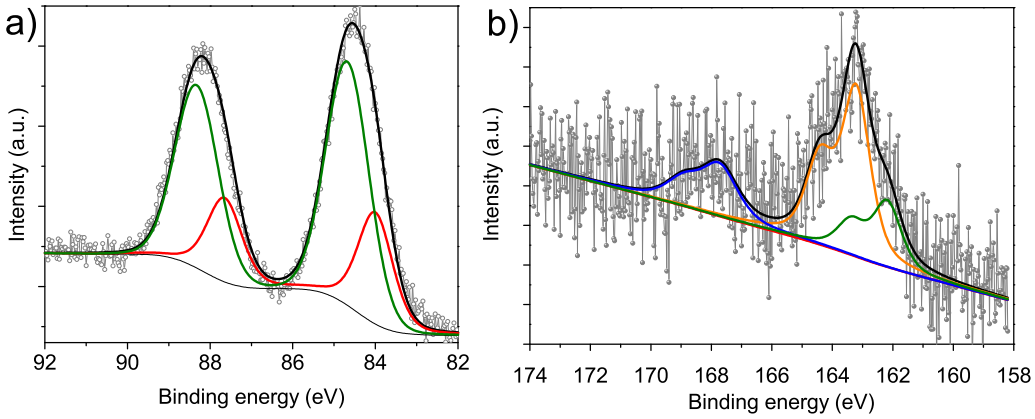

Figure S6: XPS spectra of the Au@Au(I)-TM nanoparticles after seven months of being sinthesized. **a)** Spectrum of the Au 4*f* region where the same components of the freshly measured particles are seen. **b)** Spectrum of the S 2*p* region. A new component of oxidized sulfur (167 eV) is observed.

References

(1) http://www.soft-imaging.net/.

(2) Wang, Z. L. *Characterization of nanophase materials*; Wiley-VCH, 2000.

(3) Stadelman, P. *JEMS-CIME-EPFL*, 2009.

(4) Martin, H.; Carro, P.; Creus, A. H.; Gonzalez, S.; Andreasen, G.; Salvarezza, R. C.; Arvia, A. J. *Langmuir* **2000**, *16*, 2915–2923.

(5) Cheney, G. E.; Fernando, Q.; Freiser, H. *J. Phys. Chem.* **1959**, *63*, 2055–2057.

(6) Zucconi, T. D.; Janauer, G. E.; Donahe, S.; Lewkowicz, C. *J. Pharm. Sci.* **1979**, *68*, 426–432.

(7) *Handbook of Chemistry and Physics*, 80th ed.; CRC Press:Boca Raton.